Dalton Transactions

ROYAL SOCIETY OF CHEMISTRY

PAPER

View Article Online
View Journal | View Issue

Cite this: *Dalton Trans.*, 2025, **54**, 1425

Selective lithium halide ion-pair sensing by a dynamic metalloporphyrin [2]rotaxane†

Jamie T. Wilmore, [a] Andrew Docker [b] and Paul D. Beer *[a]

Received 30th October 2024,
Accepted 22nd November 2024

DOI: 10.1039/d4dt03026e

rsc.li/dalton

A dynamic zinc(II) metalloporphyrin axle-containing [2]rotaxane with a heteroditopic macrocycle component is shown to selectively recognise and optically sense lithium halide (LiX) ion-pair species. ^{1}H NMR and UV-visible absorption experiments demonstrate a strong macrocycle pyridyl···Zn(II) metalloporphyrin axle interaction which results in a marked co-conformational bias in the free [2]rotaxane host system. Extensive ^{1}H NMR cation, anion and ion-pair titration experiments demonstrate the binding of lithium halide ion-pairs disrupts the inter-component mechanical bond interaction, wherein dynamic macrocycle shuttling to an axle triazole station enables co-operative axle-separated LiX ion-pair recognition and the selective optical sensing of lithium halide salts.

Introduction

The key technological roles played by simple alkali metal salts have led to significant interest in the development of supramolecular systems for their selective recognition and sensing.[1] In particular, lithium halide (LiX) salts are of significant industrial interest, in no small part due to growing global demand arising from advances in battery technology.[2] In addition, misregulation of lithium salts is implicated in a number of degenerative neurological conditions, such as Parkinson's and Alzheimer's diseases.[3,4]

Within the field of ion-pair recognition, lithium halide salts remain a particular challenge on account of the large electrostatic penalty associated with separating the small, charge dense, Li^{+} cation from its associated halide counterion.[5] To overcome this challenge, supramolecular chemists have employed heteroditopic receptors,[6–12] which contain separate cation and anion binding motifs, to give rise to both favourable electrostatic and allosteric effects to stabilise the co-bound ion-pair.[13–17] Indeed, the challenges associated with the selective recognition of lithium halides consequently translates to difficulty in the construction of systems capable of their selective sensing. We were therefore motivated by the opportunity to explore novel receptor designs and sensory mechanisms to meet this demand.

Given their superior binding selectivities and affinities over their non-interlocked host analogues,[18] utilising mechanically interlocked molecules (MIMs) in heteroditopic host design for ion-pair recognition has a number of advantages.[19] In particular, their unique topologies facilitate highly preorganised convergent binding sites, while the inherent relative motion between interlocked components, known as co-conformational dynamism, can give rise to favourable allosteric effects. Such inherent dynamic motion has previously been exploited as an innovative mechanism for enhanced ion-pair binding, wherein binding of one species preorganises the host for a second, counterion, binding event, enhancing binding affinities. Furthermore, incorporation of optical reporter groups into a dynamic rotaxane can serve as an innovative optical signalling mechanism for ion-pair binding.[20,21] However, despite this, examples of heteroditopic MIMs remain rare.[22]

While metalloporphyrins have a range of advantageous properties for ion sensing, with a Lewis acidic metal centre which displays marked photochemical and electrochemical shifts upon the binding of neutral and anionic Lewis bases,[23–26] there have been to date very few examples of metalloporphyrin-containing rotaxanes capable of exhibiting such a response to a guest binding event.[27–30]

Herein, we report a novel dynamic Zn(II) metalloporphyrin [2]rotaxane molecular shuttle, containing a heteroditopic pyridyl/isophthalamide macrocycle, wherein strong co-ordination of the macrocycle pyridyl to the metalloporphyrin axle component results in a marked co-conformational bias of the rotaxane in the absence of guest ions. Extensive cation, anion and ion-pair ^{1}H NMR binding studies demonstrate that the binding of a LiX ion-pair induces macrocycle shuttling to the [2]rotaxane triazole axle station, unmasking the vacant Zn(II) axial co-ordination site and switching-on anion recognition and sensing at the photo-active porphyrin, achieving a marked optical response (Fig. 1). This dynamic MIM allosteric effect in

[a]*Department of Chemistry, Chemistry Research Laboratory, University of Oxford, Mansfield Road, Oxford, OX1 3TA, UK. E-mail: paul.beer@chem.ox.ac.uk*
[b]*Yusuf Hamied Department of Chemistry, University of Cambridge, Lensfield Road, Cambridge, CB2 1EW, UK*

†Electronic supplementary information (ESI) available. See DOI: https://doi.org/10.1039/d4dt03026e

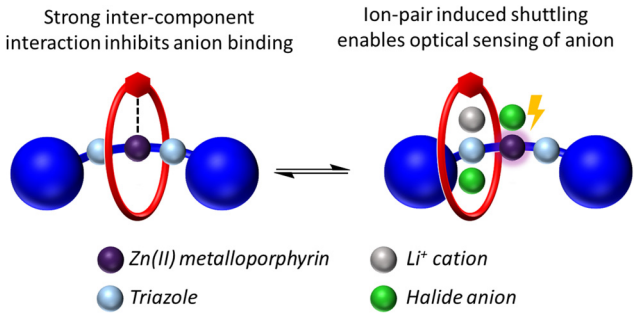

Fig. 1 Schematic depiction of ion-pair binding-induced macrocycle shuttling and anion optical response.

the presence of a co-bound LiX salt serves as a novel signalling mechanism for the detection of ion-pairs.

Results and discussion

Rotaxane synthesis

We have recently reported a series of Zn(II) metalloporphyrin rotaxanes,[30] in which a significant inter-component co-ordination interaction between the Zn(II) centre and a pyridyl macrocycle dramatically reduces the affinity of the metalloporphyrin-centre to bind a Lewis base (*i.e.* a negative allosteric effect), greatly diminishing anion binding affinity relative to non-interlocked analogues.

Building on this work, the design strategy for the target ion-pair binding rotaxane incorporated heteroditopic macrocycle **1**, containing an isophthalamide HB-donor anion binding site, previously reported for the strong binding of anions,[31] and a pyridyl group capable of both endotopic co-ordination of the axle Zn(II) metalloporphyrin centre,[32] and binding of a Li^+ cationic guest species.[33] Macrocycle **1** was prepared in accordance with a literature procedure,[31] and used in an active-metal templated (AMT) reaction using a copper(I)-catalysed alkyne–azide click (CuAAC) methodology to generate the target rotaxane (Scheme 1).[34–37] Such a methodology further affords the facile incorporation of two axle triazole motifs which have the potential to coordinate the guest Li^+ cation.[33,38]

One equivalent of macrocycle **1**, precomplexed with Cu(I), was heated with 3 equivalents of Zn(II) metalloporphyrin bis-azide **2·Zn**[39] and six equivalents of terphenyl functionalised stopper alkyne **3**,[40] in 1,2-dichloroethane at 60 °C for 3 days (Scheme 1a). Following purification by preparative thin layer chromatography, the target metalloporphyrin [2]rotaxane **4·Zn** was isolated in high yield (73%), in addition to the non-interlocked axle **5·Zn**. The rotaxane was characterised by ^{1}H and ^{13}C $\{^1$H$\}$ NMR spectroscopy, and high-resolution electrospray ionisation mass spectrometry (see ESI†).

To confirm the mechanically interlocked nature of **4·Zn**, the ^{1}H NMR spectrum of the [2]rotaxane was compared to the non-interlocked macrocycle **1** and axle **5·Zn** components (Fig. 2). In particular, the macrocycle resonances *e* and *f* and axle protons 4 and 5 displayed marked upfield shifts, likely due to the mutual effects of ring currents from the aromatic rings of both interlocked components.

Investigation of rotaxane co-conformational bias

In addition to the aforementioned diagnostic shifts, the room temperature ^{1}H NMR spectrum of **4·Zn** in $CDCl_3$ also demonstrated significant broadening suggesting slow translocation of the macrocycle along the axle relative to the NMR timescale with the system approaching the coalescence point under the conditions of Fig. 2,[41] strongly indicating a significant kinetic barrier to shuttling arising through a strong pyridyl···Zn inter-component interaction. To aid ^{1}H NMR assignment, a variable-temperature NMR study was conducted. Pleasingly, upon heating, the proton resonances of **4·Zn** became increasingly resolved (Fig. 3), due to an increase in the rate of macrocycle shuttling. Eyring analysis determined the activation parameters for macrocycle translocation $\Delta H^{\ddagger}$ = 65 kJ mol^{-1} and $\Delta S^{\ddagger}$ = 45 J K^{-1} mol^{-1}.[42] The calculated enthalpy of activation is significantly more endothermic than that calculated in our previously reported Zn(II) metalloporphyrin shuttles,[30] wherein macrocycle translocation is retarded by a pyridyl···Zn inter-component interaction (Fig. 4). These results strongly suggest **4·Zn** exhibits a similar co-conformational bias for a 'resting state' co-conformation, in which the dynamic shuttling behaviour of the macrocycle along the axle is modulated such that the macrocycle is significantly co-conformationally biased to reside over the axle metalloporphyrin group, maximising the favourable pyridyl···Zn interactions (*vide infra*). Such slowing of macrocycle translocation likely accounts for the significant broadening of the ^{1}H NMR spectrum of **4·Zn** in Fig. 2.

To confirm the significant barrier to macrocycle translocation arises through a pyridyl···Zn inter-component interaction, and not due to other effects such as the steric demand of the macrocycle passing over the porphyrin ring, the free-base rotaxane **4·H$_2$** was prepared. Stirring a CH_2Cl_2 solution of **4·Zn** with trifluoroacetic acid (TFA) afforded the free-base rotaxane **4·H$_2$** in 92% yield (Scheme 1b). As predicted, the room temperature ^{1}H NMR spectrum of **4·H$_2$** was well-resolved (ESI, Fig. S5†), demonstrating the macrocycle is able to freely translocate along the axle at room temperature, confirming the origin of the barrier to macrocycle translocation as the pyridyl···Zn interaction.

Given the significant energetic barrier to shuttling in **4·Zn**, it was of interest to calculate the percentage occupancy of the 'resting state' co-conformation. To this end, a UV-visible absorbance titration of **4·Zn** and pyridine was performed. Upon successive addition of pyridine to a $CHCl_3$ solution of **4·Zn**, a marked bathochromic shift was observed (ESI, Fig. S11†), consistent with binding of pyridine at the rotaxane's Zn(II) centre,[43,44] which is known to result in displacement of the macrocycle from the metalloporphyrin core.[30] Fitting of the bathochromic shift titration data determined a 1 : 1 host : guest binding stoichiometry, with a pyridine binding constant, K_{rot} = 645 M^{-1}, which is significantly lower than for the non-interlocked axle, K_{ax} = 7630 M^{-1}.[30] From this quantitative data, a 93% occupancy of the 'resting state' co-conformation was calculated (Table 1, see ESI†),[32] demonstrating a very high co-con-

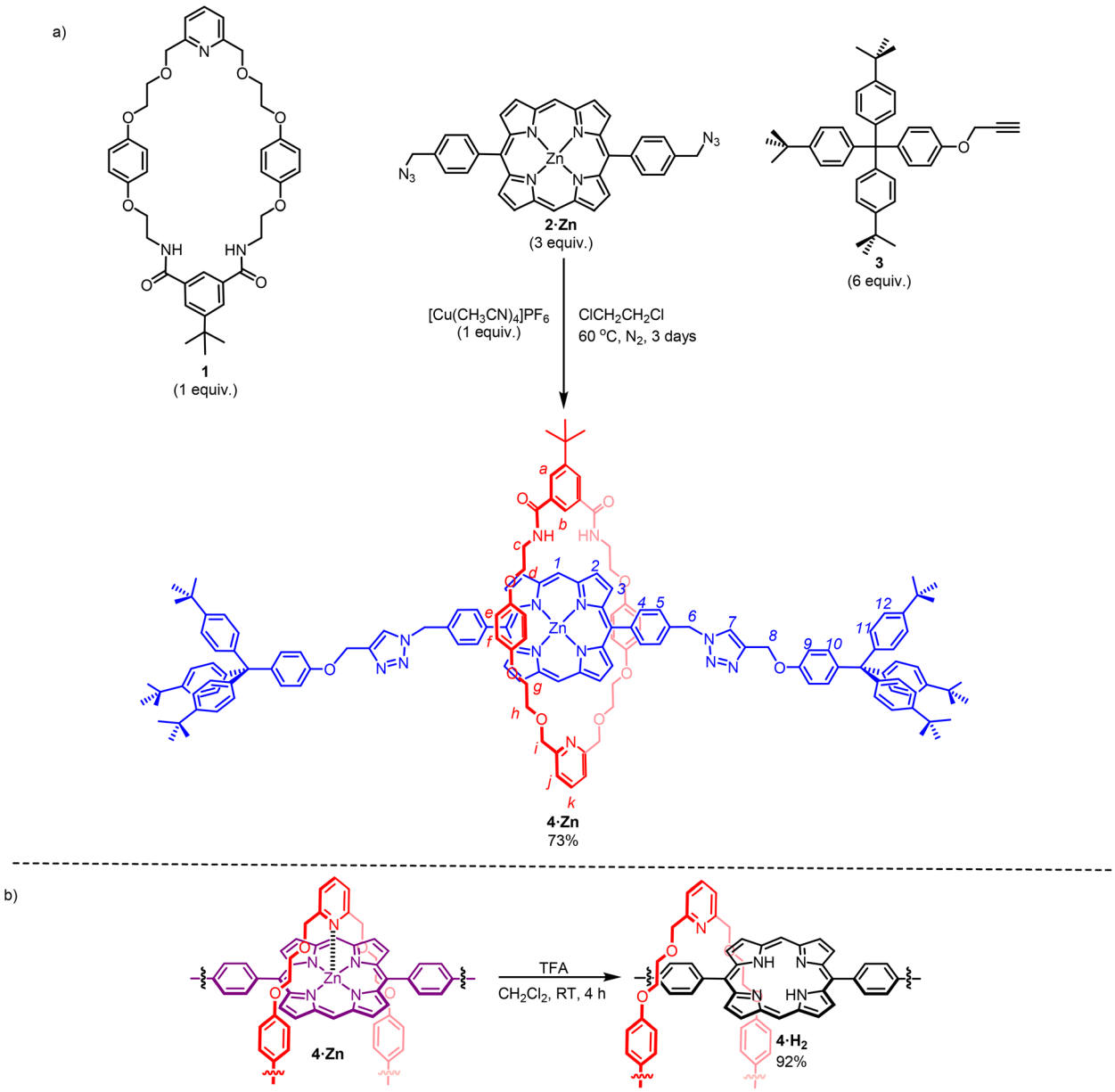

Scheme 1 (a) Synthesis of Zn(II) metalloporphyrin-containing [2]rotaxane **4·Zn**. (b) Synthesis of free-base porphyrin-containing [2]rotaxane **4·H$_2$**.

formational bias arises from the significant pyridyl···Zn(II) metalloporphyrin interaction.

^{1}H NMR anion, cation and ion-pair binding studies

Initially, the ability of **4·Zn** to bind halide anions and Li^+ was probed by a ^{1}H NMR titration study in 7 : 3 v/v $CDCl_3$: CD_3CN.‡ This organic solvent mixture ratio was selected to ensure adequate solubility of rotaxane **4·Zn**, tetra-*n*-butyl ammonium halide (TBAX) salts and $LiClO_4$ salts at NMR concentrations.

Upon addition of increasing equivalents of TBAX (X = Cl, Br) salts to **4·Zn**, marked upfield shifts were observed in porphyrin proton resonances 1, 2 and 3, whilst no significant perturbation was observed in triazole proton 7 or the macrocycle isophthalamide N*H* proton, revealing that, in the absence of co-bound Li^+, the halide anions bind exclusively at the rotaxane's Lewis acidic Zn(II) metalloporphyrin axle recognition site.

Monitoring proton 3, Bindfit analysis of the titration isotherms determined 1 : 1 stoichiometric host–guest association constants (Table 2),[45,46] where halide Lewis basicity and charge density dictates that the chloride anion is preferentially bound.

‡ ^{1}H NMR binding titrations in acetone-d_6 were attempted, however the ^{1}H NMR resonances were not well-resolved which precluded accurate fitting. Adding CD_3CN weakens the inter-component interactions (see ref. 50) and thus increases the resolution of the ^{1}H NMR spectra making them suitable for binding constant determination.

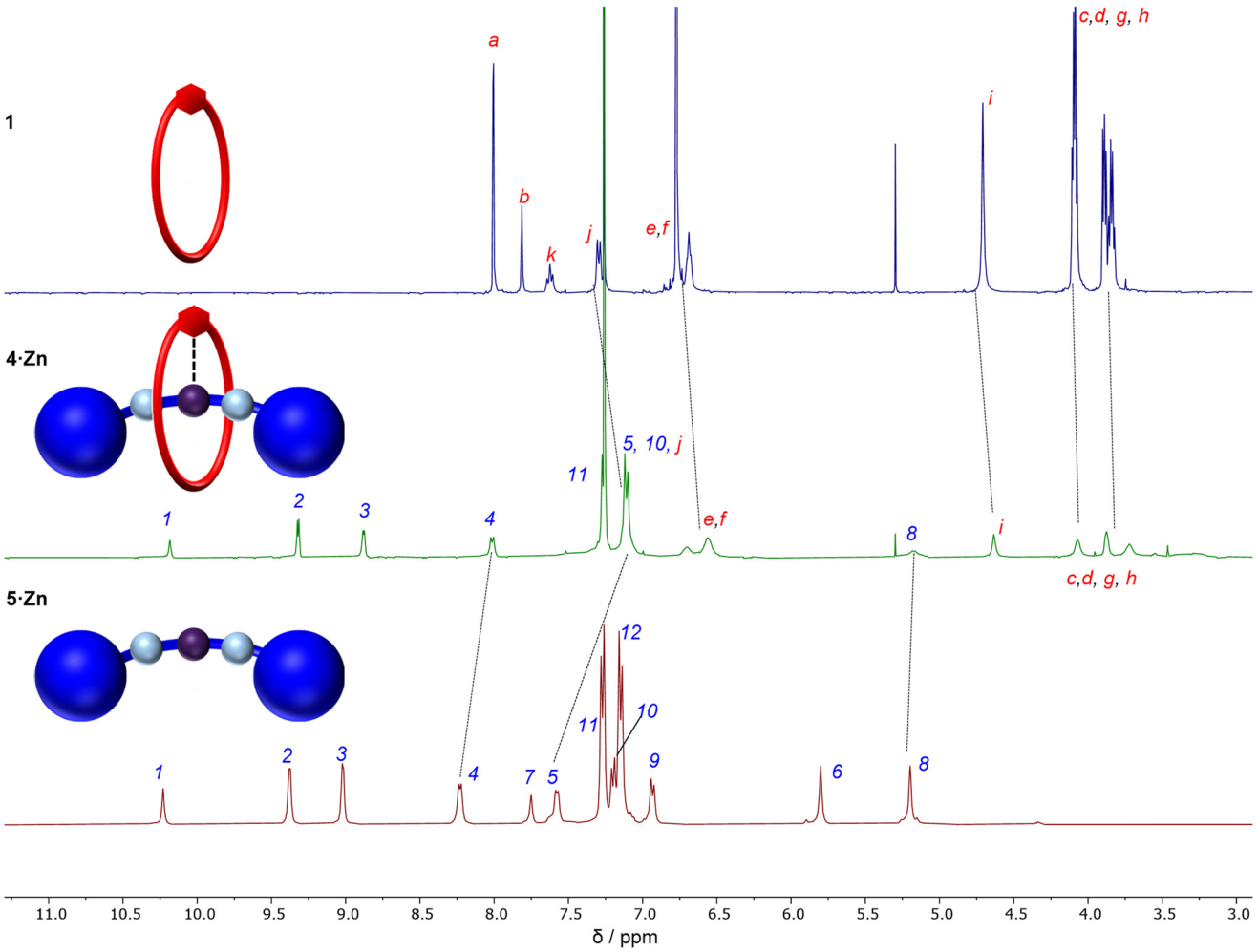

Fig. 2 Stacked ^{1}H NMR (400 MHz, 298 K, $CDCl_3$) spectra of **1**, **4·Zn** and **5·Zn**.

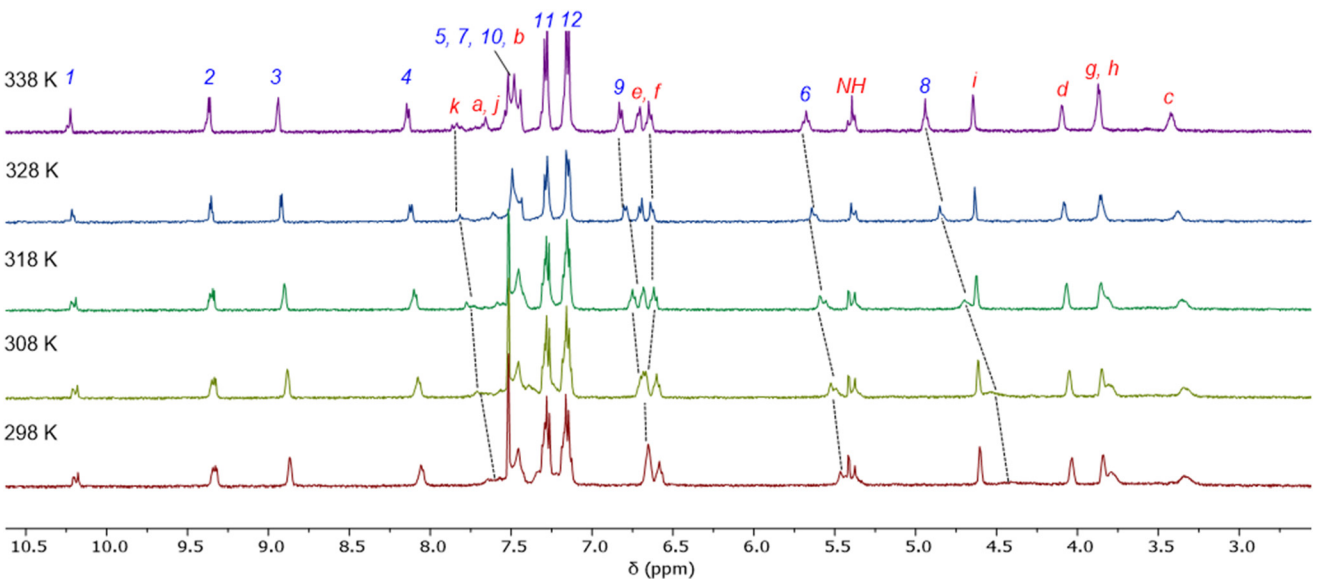

Fig. 3 Variable temperature ^{1}H NMR (500 MHz, $CDCl_3$) spectra of [2]rotaxane **4·Zn**.

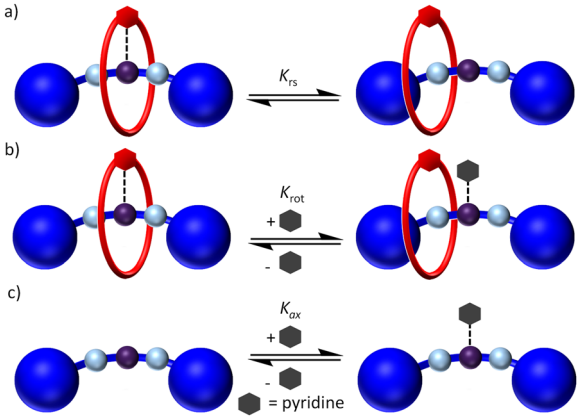

Fig. 4 Schematic depiction of the equilibria probed by optical pyridine binding studies.

Table 1 Calculated binding constants and %self-inclusion calculated from UV-visible absorbance titration of 25 mM pyridine with 7.5 μM **4·Zn** or **5·Zn** in $CHCl_3$. Errors <10%

K_{rot} (M^{-1})	K_{ax}[a] (M^{-1})	K_{rs}	% 'resting state' co-conformation
645	7630	10.8	93

[a] Taken from a previous report.[30]

Table 2 Apparent halide anion binding constants for **4·Zn** in the absence and presence of one equivalent of $LiClO_4$ (500 MHz, 298 K, 7 : 3 v/v $CDCl_3$: CD_3CN). Errors <5% SR Salt recombination observed at higher [TBACl]. NB No binding observed

	K_{app} (M^{-1})	
Anion	0 eq. Li^+	1 eq. Li^+
Cl^-	340	SR
Br^-	200	$>10^4$
I^-	NB	1750

The ^{1}H NMR titration study between $LiClO_4$ and **4·Zn** showed the macrocycle methylene proton *i* shifted sharply downfield upon Li^+ addition, consistent with the binding of a Li^+ cation in the macrocycle pyridyl binding pocket (Fig. 5). Significant perturbations were also observed in the adjacent ethylene protons *g* and *h*. Notably, a marked shift was also observed in the triazole proton 7, strongly suggesting the macrocycle had shuttled to one of the axle triazole groups of **4·Zn** to facilitate co-operative Li^+ binding between the macrocycle pyridyl and a triazole N donor atom. Bindfit analysis of the resulting binding isotherm, fitting to a 1 : 1 host guest binding stoichiometry, determined K_a = 285 M^{-1}.

Having elucidated **4·Zn** was capable of binding the Li^+ cation *via* a mechanical bond-enabled inter-component macrocycle pyridyl-axle triazole nitrogen coordination mode, attention turned to investigating the potential for the rotaxane to bind a lithium halide ion-pair. ^{1}H NMR ion-pair titration

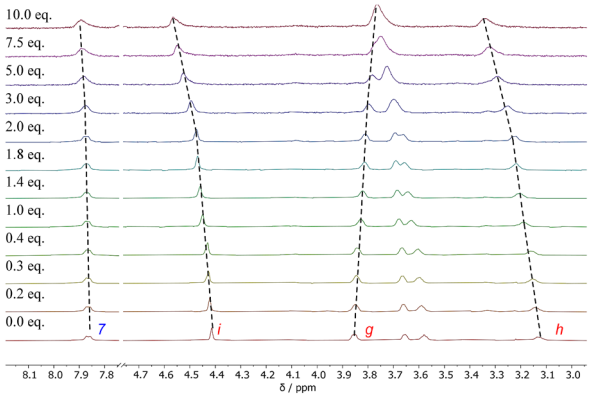

Fig. 5 Truncated ^{1}H NMR (500 MHz, 298 K, 7 : 3 v/v $CDCl_3$: CD_3CN) spectra upon successive addition of an $LiClO_4$ solution to **4·Zn**.

binding studies were performed by successive addition of TBAX solutions to an equimolar 1 mM solution of **4·Zn** and $LiClO_4$. It is noteworthy that, given the modest Li^+ cation association constant (K_a = 285 M^{-1}), only approximately 20% of the Li^+ is bound by the rotaxane host at the starting point of these experiments.

Upon addition of the respective TBAX salt, significant shifts were observed in the ^{1}H NMR spectra: the internal macrocycle phenyl proton *b* and isophthalamide N*H* proton both displayed marked downfield shifts, consistent with anion binding occurring within the isophthalamide cavity of the macrocycle. Furthermore, the axle triazole proton 7 also demonstrated significant perturbations, while only minimal changes were observed for the metalloporphyrin protons 1, 2 and 3, confirming that the halide binding event occurs at the axle triazole group. Bindfit analysis of the resultant binding isotherms (Fig. 6) enabled calculation of the apparent 1 : 1 stoichiometric halide binding constants, demonstrating very strong binding of chloride and bromide (K_{app} > 10^4 M^{-1}), while a significant enhancement in binding of the less Lewis basic I^- anion was

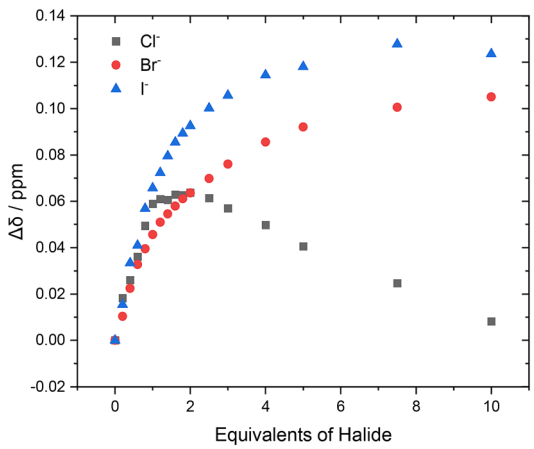

Fig. 6 ^{1}H NMR (500 MHz, 298 K, 7 : 3 v/v $CDCl_3$: CD_3CN) binding isotherms, mapping phenyl proton *b* in an equimolar solution of **4·Zn** and $LiClO_4$ upon successive additions of TBAX (X = Cl, Br, I).

also observed (Table 2). Unfortunately, at higher concentrations of Cl^- the ^1H NMR resonances returned to their original shift values and the formation of LiCl solid was observed in the ^1H NMR sample, indicating ion-pair binding was unable to overcome salt recombination, driven by the high lattice enthalpy of LiCl. Such salt recombination was not observed for LiBr or LiI, likely on account of their lower lattice enthalpies, and hence reduced driving force for salt recombination (Fig. 6).[19,47]

This observed near-quantitative LiBr ion-pair binding by rotaxane **4·Zn** evidences the high degree of co-operativity facilitated by the mechanical bond effect. Initial Li^+ binding disrupts the Zn(II)···pyridyl inter-component interaction, preorganises the macrocycle into a favourable co-conformation (allosteric effect) and polarises the axle triazole to enhance halide binding through proximal coulombic electrostatic attraction.[38]

Further evidence that halide binding enhances Li^+ binding can be observed from the continued downfield shifts of the macrocycle external pyridyl proton *k* and ethylene proton *h* upon successive Br^- addition. The significant enhancement in both Li^+ and Br^- binding occurring only when both components are present functions akin to a Boolean AND logic gate,[48,49] in which the presence of both components of the ion-pair is required to induce significant binding, resulting in macrocycle shuttling to the triazole station.

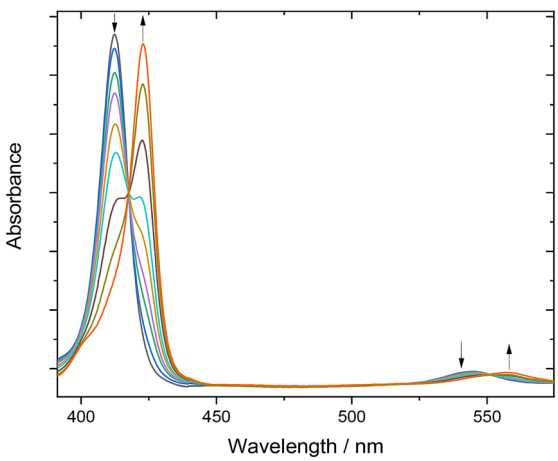

Fig. 7 UV-visible absorption spectra (2 μM, acetone) of the Soret and Q band absorptions of **4·Zn**, upon successive additions of 100 mM TBACl. Black arrows indicate directions of change.

Table 3 Calculated binding constants from UV-visible absorbance titrations of 100 mM TBAX salt with 2 μM **4·Zn**, **5·Zn** and equimolar **4·Zn**, LiTFSI and TBAX (**4·Zn·Li$^+$X$^-$**) in acetone. Errors <10%

	K_a (M^{-1})		
Anion	**4·Zn**	**5·Zn**[a]	**4·Zn·Li$^+$X$^-$**
Cl^-	190	910	910
Br^-	<20	40	45
I^-	NB	NB	NB

[a] Taken from a previous report.[30] NB No binding observed.

Optical anion and ion-pair binding studies

Preliminary optical UV-visible absorption titrations were performed with TBAX (X = Cl, Br, I) in acetone, on account of the low solubility of TBAX salts in $CHCl_3$. Upon successive additions of 100 mM solutions of TBACl or TBABr to a 2 μM solution of **4·Zn**, bathochromic shifts were observed in both the Soret and Q-band absorptions of the metalloporphyrin centre (Fig. 7). Fitting of the resulting isotherms confirmed a 1 : 1 host : guest binding stoichiometry with halide anion binding constants of significantly lower magnitude than those for the non-interlocked axle **5·Zn** (Table 3),[30] wherein the guest anion does not compete with the macrocycle pyridyl for the single vacant axial co-ordination site of the Zn(II) Lewis acidic metalloporphyrin centre. The calculated binding constants follow halide basicity trends such that $K_a(Cl^-) \gg K_a(Br^-)$, with no binding observed for I^-.[25]

Given the earlier ^1H NMR studies demonstrated binding of Li^+/X^- (X = Cl, Br) ion-pairs induces macrocycle shuttling away from the metalloporphyrin, removing the competing inter-component interaction, it was expected ion-pair binding would give rise to a positive allosteric effect (Fig. 8), recovering anion binding affinities at the porphyrin site close to those of the non-interlocked axle **5·Zn**. To this end, optical anion binding studies were performed on **4·Zn** in the presence of a co-bound ion-pair. Due to the known propensity of acetonitrile to interact with Zn(II) metalloporphyrins, perturbing the metalloporphyrin optical spectra,[50] these studies were conducted in acetone, using the acetone soluble Li^+ source lithium bis(trifluoromethane)sulfonimide (LiTFSI).

Pleasingly, the UV-visible absorption spectrum of an equimolar acetone solution of **4·Zn**, LiTFSI and TBACl demon-

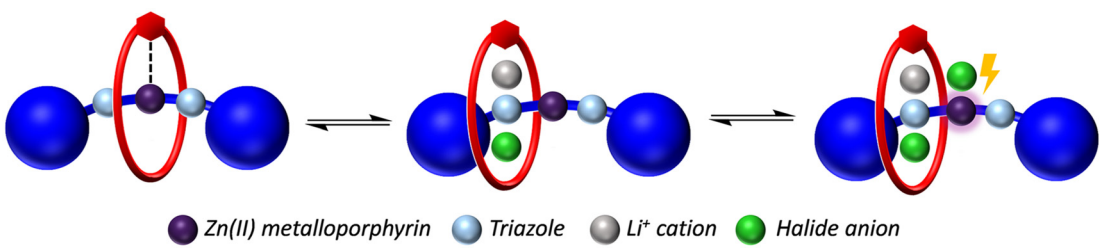

Fig. 8 Schematic depiction of ion-pair binding-induced macrocycle shuttling, removing the Zn(II)···pyridyl inter-component interaction, enhancing subsequent anion sensing by a positive allosteric effect.

strated a 2 nm hypsochromic shift in the Zn(II) metalloporphyrin Soret band absorption from 413 nm to 411 nm, consistent with that seen for the non-interlocked axle **5·Zn**, strongly evidencing Li^+ binding was inducing macrocycle translocation away from the Zn(II) centre, removing the pyridyl···Zn(II) inter-component interaction in **4·Zn·Li$^+$**. Based on the earlier ^{1}H NMR data, it would be expected that this interaction would be almost completely removed upon addition of Cl^- or Br^-, due to near-quantitative binding of an axle-separated ion-pair in the heteroditopic macrocycle (Fig. 8).

Upon successive additions of 100 mM solutions of TBAX (X = Cl, Br, I) to a 2 μM solution of **4·Zn·Li$^+$X$^-$** in acetone, a marked bathochromic shift in the Soret band was observed, consistent with a second halide anion binding at the Zn(II) metalloporphyrin site (Fig. 8). As for **5·Zn**, no such shift was observed upon TBAI addition, on account of the low Lewis basicity of the iodide anion. Fitting of the binding isotherms for TBACl and TBABr revealed a six- and four-fold enhancement of the Zn(II)···halide binding constant for **4·Zn·Li$^+$X$^-$** over **4·Zn** respectively (Table 3). Impressively, the measured anion binding constants for **4·Zn·Li$^+$X$^-$** are approximately equal to those for the axle **5·Zn**. Importantly, this demonstrates the introduction of a heteroditopic macrocycle provides an effective mechanism for the gating of an anion binding site. Ion-pair binding disrupts the competing macrocycle-axle inter-component interaction, inducing co-conformational dynamism to facilitate translocation of the macrocycle away from the Zn(II) centre which results in complete recovery of anion binding affinity at the metalloporphyrin axle station.

Conclusions

In conclusion, a novel dynamic [2]rotaxane, **4·Zn**, containing a Zn(II) metalloporphyrin axle and a heteroditopic macrocycle was synthesised in high yield *via* AMT mechanical bond formation. Importantly, the mechanically interlocked topology of **4·Zn** enables a marked inter-component interaction between the macrocycle pyridyl nitrogen atom and the vacant axial co-ordination site of the Zn(II) metalloporphyrin, resulting in a significant 'resting state' co-conformational bias (>90%) in which the macrocycle resides over the metalloporphyrin core. Such high co-conformational fidelity serves to 'gate' the Lewis acidic axial co-ordination site of the Zn(II) metalloporphyrin, leading to significantly reduced halide anion binding affinities for **4·Zn** over the non-interlocked axle **5·Zn**.

Detailed ^{1}H NMR binding studies reveal that lithium cation and lithium cation-halide anion ion-pair complexation disrupts the inter-component mechanical bond interaction, resulting in the shuttling of the macrocycle to the axle's triazole group station.

While **4·Zn** binds the individual Li^+ cation or halide anions relatively weakly, axle-separated lithium-halide LiX ion-pair complex formation through convergent binding between the rotaxane's heteroditopic macrocycle and the axle triazole motif is very strong. Thus, in the presence of a co-bound ion-pair, the Zn(II) metalloporphyrin axle co-ordination site is left vacant for the subsequent binding of an anionic guest, and hence facilitates anion sensing. Impressively, in the case of the strongly bound lithium chloride ion pair, this positive allosteric effect leads to complete recovery of rotaxane anion binding affinity to that of the non-interlocked axle **5·Zn**. Such an AND logic mechanism demonstrates the potential application of molecular shuttles for the selective detection of ionic salts only where both components are present, with clear future applications for industrial and healthcare sensing.

Data availability

The data supporting this article have been included as part of the ESI.†

Conflicts of interest

There are no conflicts to declare.

Acknowledgements

J. T. W. thanks the EPSRC for funding (Centre for Doctoral Training in Inorganic Chemistry for Future Manufacturing (OxICFM, EP/S023828/1) and a Doctoral Prize Award (EP/W524311/1)). A. D. thanks the EPSRC for a studentship (EP/N509711/1). Andrew J. Taylor, University of Oxford, is thanked for useful discussions.

References

1 A. J. McConnell, A. Docker and P. D. Beer, *ChemPlusChem*, 2020, **85**, 1824–1841.
2 G. Martin, L. Rentsch, M. Höck and M. Bertau, *Energy Storage Mater.*, 2017, **6**, 171–179.
3 M. Niethammer and B. Ford, *Mov. Disord.*, 2007, **22**, 570–573.
4 P. Newman and M. Saunders, *Postgrad. Med. J.*, 1979, **55**, 701–703.
5 *CRC Handbook of Chemistry and Physics*, ed. J. R. Rumble, CRC Press, 2021.
6 H. Piotrowski, G. Hilt, A. Schulz, P. Mayer, K. Polborn and K. Severin, *Chem. – Eur. J.*, 2001, **7**, 3196–3208.
7 H. Piotrowski, K. Polborn, G. Hilt and K. Severin, *J. Am. Chem. Soc.*, 2001, **123**, 2699–2700.
8 J. M. Mahoney, A. M. Beatty and B. D. Smith, *Inorg. Chem.*, 2004, **43**, 7617–7621.
9 Q. He, N. J. Williams, J. H. Oh, V. M. Lynch, S. K. Kim, B. A. Moyer and J. L. Sessler, *Angew. Chem., Int. Ed.*, 2018, **57**, 11924–11928.

10 Z. Kokan and M. J. Chmielewski, *J. Am. Chem. Soc.*, 2018, **140**, 16010–16014.
11 Y. C. Tse, A. Docker, Z. Zhang and P. D. Beer, *Chem. Commun.*, 2021, **57**, 4950–4953.
12 K.-I. Hong, H. Kim, Y. Kim, M.-G. Choi and W.-D. Jang, *Chem. Commun.*, 2020, **56**, 10541–10544.
13 B. Qiao, A. Sengupta, Y. Liu, K. P. McDonald, M. Pink, J. R. Anderson, K. Raghavachari and A. H. Flood, *J. Am. Chem. Soc.*, 2015, **137**, 9746–9757.
14 T. Bunchuay, A. Docker, U. Eiamprasert, P. Surawatanawong, A. Brown and P. D. Beer, *Angew. Chem., Int. Ed.*, 2020, **59**, 12007–12012.
15 A. J. Taylor, A. Docker and P. D. Beer, *Chem. – Asian J.*, 2023, **18**, e202201170.
16 A. Docker, I. Marques, H. Kuhn, Z. Zhang, V. Félix and P. D. Beer, *J. Am. Chem. Soc.*, 2022, **144**, 14778–14789.
17 A. Docker, Y. C. Tse, H. M. Tay, Z. Zhang and P. D. Beer, *Dalton Trans.*, 2024, **53**, 11141–11146.
18 J. T. Wilmore and P. D. Beer, *Adv. Mater.*, 2024, **36**, 2309098.
19 H. M. Tay, Y. C. Tse, A. Docker, C. Gateley, A. L. Thompson, H. Kuhn, Z. Zhang and P. D. Beer, *Angew. Chem., Int. Ed.*, 2023, **62**, e2022147.
20 H. M. Tay, A. Docker, Y. C. Tse and P. D. Beer, *Chem. – Eur. J.*, 2023, **29**, e202301316.
21 C. Gao, Z.-L. Luan, Q. Zhang, S. Yang, S.-J. Rao, D.-H. Qu and H. Tian, *Org. Lett.*, 2017, **19**, 1618–1621.
22 A. Arun, H. M. Tay and P. D. Beer, *Chem. Commun.*, 2024, **60**, 11849–11863.
23 D. P. Cormode, M. G. B. Drew, R. Jagessar and P. D. Beer, *Dalton Trans.*, 2008, 6732–6741.
24 D. P. Cormode, S. S. Murray, A. R. Cowley and P. D. Beer, *Dalton Trans.*, 2006, 5135–5140.
25 L. C. Gilday, N. G. White and P. D. Beer, *Dalton Trans.*, 2013, **42**, 15766–15773.
26 L. C. Gilday, N. G. White and P. D. Beer, *Dalton Trans.*, 2012, **41**, 7092–7097.
27 M. Wolf, A. Ogawa, M. Bechtold, M. Vonesch, J. A. Wytko, K. Oohora, S. Campidelli, T. Hayashi, D. M. Guldi and J. Weiss, *Chem. Sci.*, 2019, **10**, 3846–3853.
28 X. Ma, J. Zhang, J. Cao, X. Yao, T. Cao, Y. Gong, C. Zhao and H. Tian, *Chem. Sci.*, 2016, **7**, 4582–4588.
29 Y. C. Tse, R. Hein, E. J. Mitchell, Z. Zhang and P. D. Beer, *Chem. – Eur. J.*, 2021, **27**, 14550–14559.
30 J. T. Wilmore, Y. C. Tse, A. Docker, C. Whitehead, C. K. Williams and P. D. Beer, *Chem. – Eur. J.*, 2023, **29**, e202300608.
31 A. Brown, T. Lang, K. M. Mullen and P. D. Beer, *Org. Biomol. Chem.*, 2017, **15**, 4587–4594.
32 S. W. Hewson and K. M. Mullen, *Org. Biomol. Chem.*, 2018, **16**, 8569–8578.
33 V. K. Munasinghe, H. M. Tay, D. Manawadu, J. Pancholi, Z. Zhang and P. D. Beer, *Dalton Trans.*, 2024, **53**, 14219–14225.
34 S. M. Goldup, D. A. Leigh, P. J. Lusby, R. T. McBurney and A. M. Z. Slawin, *Angew. Chem., Int. Ed.*, 2008, **47**, 3381–3384.
35 J. Berná, S. M. Goldup, A.-L. Lee, D. A. Leigh, M. D. Symes, G. Teobaldi and F. Zerbetto, *Angew. Chem., Int. Ed.*, 2008, **47**, 4392–4396.
36 S. M. Goldup, D. A. Leigh, T. Long, P. R. McGonigal, M. D. Symes and J. Wu, *J. Am. Chem. Soc.*, 2009, **131**, 15924–15929.
37 V. Aucagne, J. Berná, J. D. Crowley, S. M. Goldup, K. D. Hänni, D. A. Leigh, P. J. Lusby, V. E. Ronaldson, A. M. Z. Slawin, A. Viterisi and D. B. Walker, *J. Am. Chem. Soc.*, 2007, **129**, 11950–11963.
38 V. K. Munasinghe, J. Pancholi, D. Manawadu, Z. Zhang and P. D. Beer, *Chem. – Eur. J.*, 2022, **28**, e202201209.
39 D. A. Roberts, T. W. Schmidt, M. J. Crossley and S. Perrier, *Chem. – Eur. J.*, 2013, **19**, 12759–12770.
40 A. Tron, P. J. Thornton, M. Rocher, H.-P. Jacquot de Rouville, J.-P. Desvergne, B. Kauffmann, T. Buffeteau, D. Cavagnat, J. H. R. Tucker and N. D. McClenaghan, *Org. Lett.*, 2014, **16**, 1358–1361.
41 Y. Matsuoka, Y. Mutoh, I. Azumaya, S. Kikkawa, T. Kasama and S. Saito, *J. Org. Chem.*, 2016, **81**, 3479–3487.
42 H. Eyring, *J. Chem. Phys.*, 1935, **3**, 107–115.
43 L. Favereau, A. Cnossen, J. B. Kelber, J. Q. Gong, R. M. Oetterli, J. Cremers, L. M. Herz and H. L. Anderson, *J. Am. Chem. Soc.*, 2015, **137**, 14256–14259.
44 A. S. Hinman and B. J. Pavelich, *J. Electroanal. Chem.*, 1989, **269**, 53–61.
45 **https://supramolecular.org**, Bindfit v 0.5.
46 D. Brynn Hibbert and P. Thordarson, *Chem. Commun.*, 2016, **52**, 12792–12805.
47 A. Docker and H. M. Tay, *Chem. – Eur. J.*, 2024, e202402844, DOI: **10.1002/chem.202402844**.
48 A. P. de Silva and N. D. McClenaghan, *Chem. – Eur. J.*, 2004, **10**, 574–586.
49 M. Ahmad, T. G. Johnson, M. Flerin, F. Duarte and M. J. Langton, *Angew. Chem., Int. Ed.*, 2024, **63**, e202403314.
50 R. Díaz-Torres and S. Alvarez, *Dalton Trans.*, 2011, **40**, 10742–10750.